Second-Sphere and Outer-Sphere Proton Relaxation of Paramagnetic Complexes: From EPR to NMRD

J. W. Chen,*,†,§ R. L. Belford,†,§ and R. B. Clarkson‡,§

Department of Chemistry, Department of Veterinary Clinical Medicine, College of Medicine, University of Illinois at Urbana−Champaign, Urbana, Illinois 61801

Received: January 31, 1997; In Final Form: December 1, 1997

Magnetic resonance imaging often utilizes paramagnetic contrast agents (PCAs) to increase contrast between adjacent tissues. PCAs enhance the contrast by increasing the spin−lattice proton relaxation rate through processes known as inner-sphere, second-sphere, and outer-sphere mechanisms. Past studies on PCAs often described relaxation rates that are not caused by inner-sphere processes as outer-sphere, since comparatively little is known about second-sphere water. Utilizing vanadyl complexes (ethylenediaminetetraacetate (EDTA) and diethylenetriaminepentaacetate (DTPA)) that do not have an inner-sphere proton relaxation contribution and those with similar functional groups of different sizes, we find that the outer-sphere model does not adequately describe the relaxivity profiles. The observed relaxivity profiles are, however, consistent with a model that includes both second-sphere and outer-sphere contributions. Vanadyl ethoxybenzyl-diethylenetriaminepentaacetate (VOEOB-DTPA) exhibited relaxivity similar to that of DTPA, even though it is larger. This is attributed to a hydrophobic moiety on EOB-DTPA that prevents protons from binding to the second coordination sphere. The combined model developed for the vanadyl complexes is used to simulate the gadolinium triethylenetetraaminehexaacetate (GdTTHA) proton NMRD profile, and the results are extrapolated to deconvolute GdDTPA and GdEOB-DTPA proton NMRD profiles into inner-sphere, second-sphere, and outer-sphere contributions. We find that the second-sphere mechanism is significant and may contribute about 30% of the relaxivity in GdDTPA and about 10% in GdEOB-DTPA.

1. Introduction

The motion of paramagnetic complexes near solvent protons creates a local fluctuating magnetic field that increases the efficiency of proton relaxation. This property of paramagnetic species is usually utilized in contrast-media-enhanced magnetic resonance imaging (MRI) to increase the signal intensity (as in T_1 imaging) or to decrease the signal intensity (as in T_2 imaging). Following the administration of a paramagnetic contrast agent (PCA), the signal intensity of the targeted tissue becomes different from adjacent tissues that are not targeted by the contrast agent. This provides a means by which a particular tissue type may be identified or distinguished from adjacent tissues that might otherwise not be sufficiently distinct in noncontrast-media-enhanced imaging. A rational design of paramagnetic contrast agents requires that the potential agent possess not only high proton relaxation enhancement but also specificity for different tissue types (as well as low toxicity and excretability). To be able to incorporate these features into a contrast agent, one should understand and exploit the relationship between chelate structure, which relates to an agent's ability to target, and the dynamics processes, which contribute to the efficacy of the proton relaxation.

The rotational dynamics of a paramagnetic agent usually modulate the proton relaxation enhancement of typical small-chelate paramagnetic contrast agents such as GdDTPA.[1,2] For such agents, the rotational correlation time (τ_R) is the most significant contributor to the inner-sphere (protons exchange within the first coordinate sphere of the agent) and the second-sphere (protons hydrogen-bonded to the second coordination sphere of the agents) proton relaxation processes at magnetic field strengths used in clinical applications ($B_0 > 1$ T). The selective study of model agents without inner-sphere contributions can offer insights into the role the second-sphere process plays in proton relaxation and can help to uncover the relationship between structure and second-sphere proton relaxation. For this to be accomplished, two types of data must be obtained: the rotational correlation time, τ_R, and the proton relaxation profile without inner-sphere contributions. These data must be measured for chelates with structural similarities so as to establish a systematic comparison of the relaxation process and to relate the chelate structure to the second-sphere proton relaxation.

The proton relaxation profiles can be obtained from nuclear magnetic resonance dispersion (NMRD) studies and will be the focus of part II of this paper. In part I we are concerned with the measurements of the rotational correlation times. Electron paramagnetic resonance (EPR) is an excellent technique to study dynamics of paramagnetic species. However, the paramagnetic ion used in clinical contrast agents, Gd^{3+}, possesses nuclei having either no magnetic moment (69.6%) or weak moments (30.4%) and is virtually isotropic in the Zeeman term at X-band. This makes Gd^{3+} very insensitive to motion. Chen et al. recently used a substitute paramagnetic ion, vanadyl (VO^{2+}), for the study of rotational dynamics of contrast agents and verified that the sizes of the vanadyl complexes are similar to

* To whom correspondence should be addressed. E-mail: jwcj@uiuc.edu.
† Department of Chemistry.
‡ Department of Veterinary Clinical Medicine.
§ College of Medicine.

S1089-5639(97)00406-4 CCC: $15.00
Published on Web 02/28/1998

their gadolinium analogues.[2] Since the pioneering work by Wilson and Kivelson[3] on vanadyl ion (VO^{2+}) dynamics, advances in both theory and computational tools have enabled extremely accurate simulations of the vanadyl EPR spectra.[2,4] Since vanadyl possesses very anisotropic hyperfine (**A**) and Zeeman (**g**) matrixes as well as a large nuclear moment ($I = 7/2$), it is very sensitive to small changes in the motion; consequently, accurate rotational correlation times can be obtained. The τ_Rs measured from EPR can be used to aid the fitting of the NMRD profiles. In addition, vanadyl, having at most five coordination sites, does not have any site for inner-sphere water when complexed with the hexadentate ethylenediaminetetraacetate (EDTA), the octadentate diethylenetriaminepentaacetate (DTPA), and the octadentate ethoxybenzyl-DTPA (EOB-DTPA). Therefore, since these complexes have no inner-sphere contribution, they are ideal for studying second- and outer-sphere mechanisms without inner-sphere complications.

At this point it is advantageous to describe briefly the theories that are commonly used in analyzing the NMRD profiles. Inner-sphere proton relaxation enhancement is due to protons bound to the first coordination sphere of the contrast agent. The Solomon−Bloembergen (SB) equations[5,6] have often been used to simulate inner-sphere relaxivity data

$$\frac{1}{T_1} = \frac{[\mathrm{M}]}{[\mathrm{M_p}]} \frac{q}{T_{1M} + \tau_M}$$

$$\mathrm{T}_{1M}^{-1}\,(\text{dipolar}) = \frac{2}{15}\left(\frac{\mu_0}{4\pi}\right)^2 \left(\frac{\gamma_I g \mu_B}{r^3}\right)^2 S(S+1)\left[\frac{7\,\tau_\mathrm{C}}{1+\omega_S^2\,\tau_\mathrm{C}^2} + \frac{3\tau_\mathrm{C}}{1+\omega_I^2\,\tau_\mathrm{C}^2}\right]$$

$$T_{1\mathrm{M}}^{-1}\,(\text{contact}) = \frac{2}{3} S(S+1)\left(\frac{\mathrm{A}_S}{\hbar}\right)^2 \frac{\tau_\mathrm{e}}{1+\omega_S{}^2\,\tau_\mathrm{C}^2} \qquad (1)$$

where q is the number of water ligands per metal ion, $[M]$ is the concentration of the paramagnetic contrast agent, $[M_p]$ is the concentration of water (55.6 mol/liter), γ_I is the nuclear gyromagnetic ratio, μ_0 is the permeability of vacuum, μ_B is the Bohr magneton, S is the electronic spin, ω_S and ω_I are the corresponding electron and nuclear Larmor frequencies, T_{1M} is the longitudinal relaxation time of inner-sphere coordinated protons, g is the electronic g-factor (assumed to be isotropic), r is the proton−metal ion distance, and A_S is the nuclear-electron hyperfine coupling constant. The correlation times τ_C and τ_e are defined as follows

$$\frac{1}{\tau_\mathrm{C}} = \frac{1}{\tau_\mathrm{R}} + \frac{1}{\tau_M} + \frac{1}{\tau_S}$$

$$\frac{1}{\tau_\mathrm{e}} = \frac{1}{\tau_M} + \frac{1}{\tau_S} \qquad (2)$$

where τ_R is the rotational correlation time for the entire agent-proton complex, τ_M is the residence lifetime of the bound water protons, and τ_S is the electronic spin relaxation time. In dilute aqueous solutions the electronic spin−lattice and the electronic spin−spin relaxation times are approximately equal;[1,7] therefore, T_{1e} is assumed to be equal to T_{2e} in this study.

It should be mentioned at this point that the Solomon−Bloembergen theory has assumptions that may limit its validity to certain systems, and these limitations have been well described by Kowalewski et al.[8] The relevant violations that may be applicable to our systems will be presented in the discussion below.

The Solomon−Bloembergen theory can also be applied to describe second-sphere proton relaxation enhancement, in which protons are hydrogen-bonded to the contrast agent and relax via a dipole−dipole interaction with the paramagnetic species. Consequently, only the dipolar term of eq 1 applies to second-sphere proton relaxation. A second-sphere process was originally proposed for fluoromethemoglobin,[9] and has also been suggested to account for the relaxivity of native transferrin.[10] Here, to differentiate between first and second sphere parameters, the relevant parameters are primed to indicate second-sphere parameters (e.g. τ_M', q', r').

Outer-sphere proton relaxation enhancement, due to protons diffusing past the agent, is most often described by translational diffusion. The translationally modulated outer-sphere diffusion contribution to T_1, based upon a rigid-sphere model (Hwang and Freed model),[7,11,12] is:

$$\frac{1}{T_1}\left(\frac{32\pi}{405}\right)\gamma_I^2\,\gamma_S^2\hbar^2\left(\frac{\mu_0}{4\pi}\right)^2 S(S+1)\frac{N_\mathrm{A}[M]}{aD}[3j(\omega_I) + 7j(\omega_S)]$$

$$j(\omega) = \mathrm{Re}\{[1 + 1/4(i\omega\tau + \tau/\tau_S)^{1/2}]/[1 + (i\omega\tau + \tau/\tau_S)^{1/2} + 4/9(i\omega\tau + \tau/\tau_S) + 1/9(i\omega\tau + \tau/\tau_S)^{3/2}]\}$$

$$\tau = 3\tau_D = a^2/D \qquad (3)$$

where a is the distance of closest approach between the solvent protons and the paramagnetic complex, N_A is Avogadro's number, and D is the sum of the diffusion coefficients for the solvent protons and the agent.

Previous studies focused on paramagnetic agents that have a large inner-sphere contribution, thus making the study of second-sphere and outer-sphere mechanisms difficult. Moreover, since relatively little is known about second-sphere effects, the relaxivity not accounted for by the inner-sphere model often was attributed entirely to translationally modulated outer-sphere relaxation (referred to as outer-sphere).[13,14] Nonetheless, several authors have suggested that the second-sphere mechanism may not be negligible.[2,15,16] Therefore, a clearer understanding of second-sphere effects would (1) allow a more physically reasonable analysis of the relaxation data and (2) aid in the design of future MRI contrast agents.

We report here the utilization of these model complexes to study second-sphere and outer-sphere mechanisms. In part I of the Results and Discussions section, we discuss the variable temperature EPR study of these complexes. In part II, we apply the EPR findings in part I to aid in the simulation of the vanadyl complexes' NMRD profiles. These profiles can be (1) compared with each other to examine the relationship between structure and second- and outer-sphere contributions and (2) simulated under a second-sphere model (SB) and/or an outer-sphere model (HF) to examine the suitability of these theories for describing the relaxation behavior of these complexes. In part III, we show how the vanadyl data can be useful in understanding gadolinium complexes.

The chelating agents chosen are shown in Figure 1. They were chosen not only because they are chelates of clinically interesting gadolinium agents, but also because they increase in size from EDTA to DTPA to EOB-DTPA and share many structural similarities.

Looking at the structures of these chelates (Figure 1), one sees that they all share one feature: the presence of carboxylic groups. At pH = 7.4, these carboxylic groups will donate their

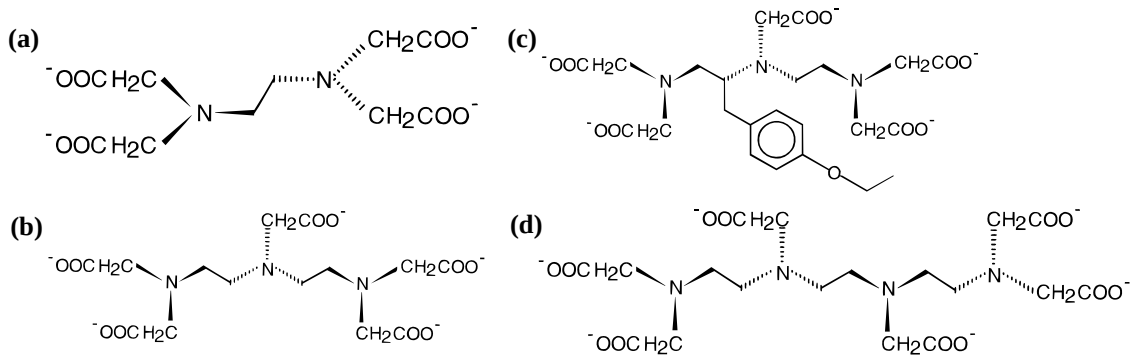

Figure 1. Structures of the chelates used in this work. Note that EDTA, DTPA, and TTHA are successive expansions of the same basic functional groups. Also note that DTPA and EOB-DTPA are identical except that EOB-DTPA contains an aromatic moiety.

protons and form anions. These negative charges and the electron-dense oxygens can potentially attract water protons and form hydrogen bonds. This should be true for both vanadyl and gadolinium complexes; in the vanadyl case, the vanadyl oxygen can also attract additional water protons. Therefore, it is reasonable to hypothesize that second-sphere protons may account for part of the so-called "outer-sphere" relaxation and potentially may confer significant relaxation to the solvent protons.

2. Materials and Methods

2.1. Chemical Preparation. All the chemicals of the highest grade were obtained from Aldrich unless otherwise indicated. The stock vanadyl sulfate solutions were prepared from deionized water and purged with argon to prevent oxidation of the vanadyl ion. Sample solutions were prepared by combining in a 1:1.2 ratio the stock vanadyl sulfate solution and the powdered chelates. EDTA and DTPA were obtained from Aldrich, TTHA was purchased from Sigma, and EOB-DTPA was supplied by Schering, AG. Sodium bicarbonate (5% solution) was used to raise the pH to physiological pH (= 7.4). *N* -(2-hydroxyethyl)-piperazine-*N*′-2-ethanesulfonic acid (HEPES) buffer was added to prevent the formation of vanadyl hydroxide[20] and to buffer the solutions. The final solutions were again purged with argon. The final concentrations were approximately 3 mM for EPR experiments and 5 mM for the NMRD experiments. Solution concentration was determined by plasma emission spectroscopy on a Perkin-Elmer Model P2000.

2.2. Spectroscopy. 2.2.1. UV/Vis Spectroscopy. UV/vis spectra were taken on all samples immediately following preparation and preceding the actual EPR experiment (in cases where time did not allow experiments to be performed immediately after preparation). All samples exhibited the characteristic two peak spectra for EDTA-like chelates complexed to vanadyl[20] to indicate that chelation was complete. The two peaks are at 586 nm (all complexes) and at 776 nm (EDTA), 772 nm (DTPA), 772 nm (TTHA), and 770 nm (EOB-DTPA). The ratios of the two peaks were approximately 0.84:1 (586 nm:770 nm). Our data indicate that these vanadyl complexes, when stored under argon and refrigerated, maintained the same optical absorbance weeks after preparation.

2.2.2. EPR Spectroscopy. Variable-temperature EPR measurements were taken on a Varian X-band spectrometer (12 in. magnet) with a TE_{102} cavity. VOEDTA and VODTPA solutions were held in an aqueous flat cell, while VOEOB-DTPA was held in a quartz tube with a 1 mm inner diameter. Sample temperatures were regulated by flowing gaseous nitrogen precooled by liquid nitrogen through a Varian variable-temperature controller and measured by a thermocouple placed near the top of the cavity. The measured temperature then was calibrated from a temperature calibration curve derived by placing thermocouples both in the center and at the top of the cavity. A standard field calibration utilizing a DTM-141 digital teslameter also was performed.

2.2.3. NMRD Relaxometry. Variable-temperature NMRD experiments were performed on a Koenig-Brown IBM field cycling relaxometer (type blue) located in the Biomedical Magnetic Resonance Laboratory at the University of Illinois at Urbana−Champaign. Experiments were performed both on the samples to find the overall relaxation rate and on the blank saline solution to obtain the diamagnetic contribution to relaxation since

$$\frac{1}{T_{1p}} = \frac{1}{T_1} - \frac{1}{T_{1d}} \tag{4}$$

where T_1 is the relaxation rate of the sample solution measured by NMRD, T_{1d} is the diamagnetic contribution to the relaxation rate, and T_{1p} is the paramagnetic contribution to the relaxation rate. $1/T_{1p}$ normalized to concentration (usually to 1 mM) is called relaxivity.

2.3. Computation. For more details on the computation methods and the software used, please consult Chen et al. and references contained therein.[2] All the software mentioned here may be obtained via anonymous ftp at the Illinois EPR Research Center.[21]

2.3.1. EPR Simulations. The powder pattern computation to derive the **A**-matrix and **g**-matrix employed SIMPOW, a sibling program of QPOW,[22,25] Motionally modulated spectral simulations used EPRLF by Budil et al.,[2,23,24] a family of programs utilizing the stochastic Liouville equations that include nonsecular contributions in the spin Hamiltonian. FIT, an automatic fitting program incorporating the EPRLF simulation engine and based on Brent's method[26] of parabolic interpolation was developed to aid and expedite the fitting process.

2.3.2. NMRD Simulations. A multidimensional fitting program (NMRD version 1.5) based on the simplex method[27] for the Solomon−Bloembergen equations (eq 1) and the Hwang and Freed equations (eq 3) was written to simulate the NMRD profiles. Because of the complexity of these equations, we have carefully verified the results of our programming with published work as well as comparing to manual computational results performed utilizing a Unix symbolic calculator with arbitrary precision, CALC, version 2.9.3t8.

The electron relaxation for vanadyl complexes and gadolinium complexes is taken to be described by

TABLE 1: Rigid-Limit-A and g-Matrixes for VOEDTA, VODTPA, VOTTHA, and VOEOB-DTPA

complex	$\mathbf{A}_{xx}{}^a$ (MHz)	$\mathbf{A}_{yy}{}^a$ (MHz)	$\mathbf{A}_{zz}{}^a$ (MHz)	$\mathbf{g}_{xx}$	$\mathbf{g}_{yy}$	$\mathbf{g}_{zz}$
VOEDTA	−183.4	−169.5	−501.2	1.981	1.978	1.945
VODTPA	−186.1	−172.0	−508.2	1.980	1.978	1.944
VOTTHA	−186.5	−169.4	−503.8	1.979	1.977	1.943
VOEOB-DTPA	−187.6	−169.7	−502.9	1.981	1.978	1.943

[a] The values of **A** can be converted from megahertz to gauss with MHz/G = $g_{\text{eff}}\beta/h$, where g_{eff} is the **g**-value along the direction concerned.[32]

$$\frac{1}{\tau_S} = \frac{1}{5\tau_{SO}}\left(\frac{1}{1+\omega_S^2\tau_V^2} + \frac{4}{1+4\omega_S^2\tau_V^2}\right) \qquad (5)$$

For gadolinium, this is the familiar Bloembergen−Morgan[28,29] modification to eq 1, the Solomon−Bloembergen equations, where τ_V is the distortion of the zero-field structure due to collision. Equations 1 and 5 together constitute the SBM equations. Kivelson has worked out the electronic relaxation for vanadyl complexes.[30] In this model, τ_S is modulated by the anisotropic Zeeman and the hyperfine interactions and influenced by rotation.[31] Therefore, τ_V, for the vanadyl ion, is related to the viscosity and is proportional to τ_R. Here, τ_V was set to $\tau_R/4$, which is similar to the value and strategy employed by Bertini et al.[31] while τ_{SO} is the magnetic field independent part of the electronic relaxation.

Because of the large number of parameters that must be simulated, we tailored our simulation program to allow an arbitrary number of variables to be either fixed or varied. This allowed us to explore and sample as much of the parameter space as physically reasonable. Our general approach involved first sampling the parameter space and then narrowing the search space by judiciously selecting and fixing certain parameters that matched the EPR results. The best-fit set was selected and its parameters perturbed by 10% to ensure consistent convergence to the same parameter values.

3. Results and Discussion

3.1. Part I: EPR of Vanadyl Complexes. Table 1 shows the rigid-limit **g** and **A** values extracted from frozen solutions at 140 K utilizing SIMPOW. The frozen solution spectra and their respective simulations are shown in Figure 2. The vanadyl rigid-limit spectra are quite complex owing to the anisotropic **g** and **A** of this $I = 7/2$ ion. This feature allows the vanadyl **g** and **A** to be accurately determined: alterations of ±1.5 MHz in the elements of **A** and ±0.001 in the elements of **g** change the χ^2 value (to four significant figures) computed for the simulation. We observed small deviations from axial symmetry in all the complexes studied. Note that the values are similar from one complex to another, indicating that the different chelates offer nearly identical coordination environments as seen from the vanadyl ion. This is to be expected since all of these chelates are structurally similar and completely saturate all the coordination sites on the vanadyl ion. This indicates that no water can coordinate with the first coordination sphere in these complexes; thus, any proton relaxation due to the presence of these complexes must come from second-sphere and/or outer-sphere interactions.

Tables 2−5 summarize the rotational correlation times for VOEDTA, VODTPA, VOEOB-DTPA, and VOTTHA found from the simulations of their respective EPR spectra, some of which are shown in Figures 3 and 4. As would be expected from the structures and molecular sizes of these complexes,

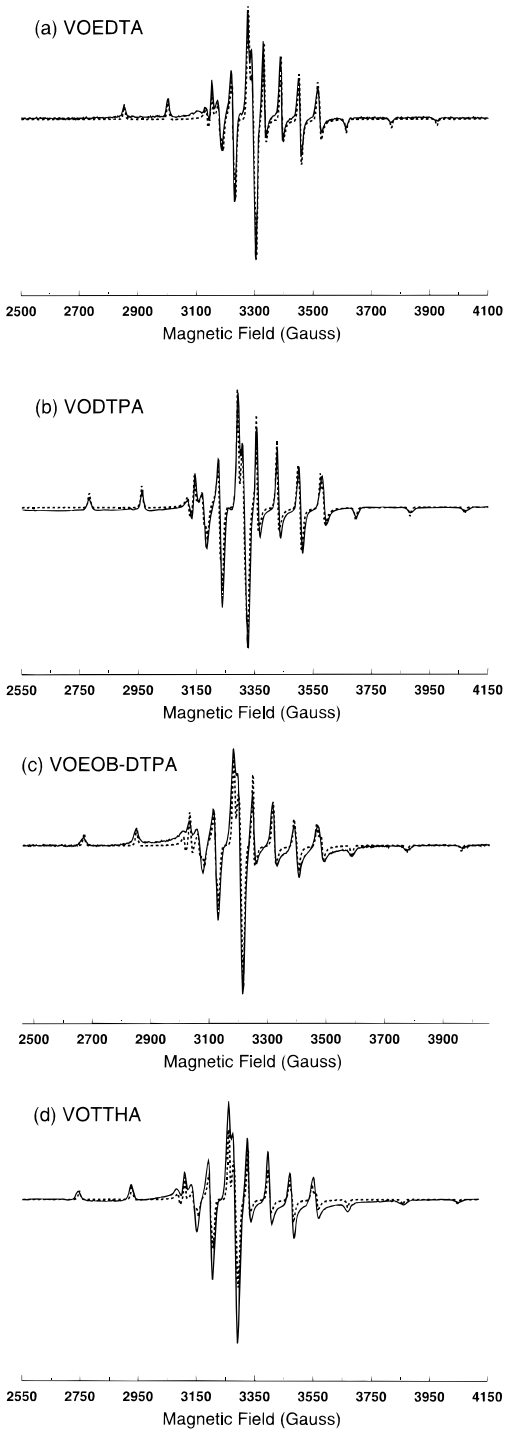

Figure 2. Frozen solution spectra and the respective best-fit simulations for the four complexes studied in part I. The solid lines are experimental spectra while the dashed lines are the best-fit simulation spectra.

VOEOB-DTPA is the slowest tumbling complex while VOEDTA is the fastest. Since the anisotropy in **g** and **A** is not completely resolved in these intermediate tumbling regimes, the simulation is slightly less sensitive than the rigid-limit simulations. Nonetheless, deviations of about 2% in τ_R are readily detected in the simulations.

It is surprising that VOTTHA is actually faster than both VODTPA and VOEOB-DTPA above 5 °C. It appears to slow substantially at lower temperatures. Q-band experiments were performed to validate the information obtained at X-band. Figure 5 shows the spectrum and its best-fit. Both Q-band and X-band results agree.

TABLE 2: Best-Fit Rotational Correlation Times (τ_R) and Residual Line Widths (α'') for VOEDTA from EPR

T (K)	τ_R (s)	α'' (G)	R^2
327	4.14×10^{-11}	2.42	0.97
300	4.78×10^{-11}	2.11	0.98
291	6.17×10^{-11}	3.70	0.99
288	8.68×10^{-11}	2.04	0.99
281	1.00×10^{-10}	2.99	0.99
276	1.13×10^{-10}	1.39	0.99
271	1.56×10^{-10}	2.85	0.99
266	3.56×10^{-09}	2.24	0.96
261	7.55×10^{-09}	1.81	0.98
257	1.04×10^{-08}	2.27	0.96

TABLE 3: Best-Fit Rotational Correlation Times (τ_R) and Residual Line Widths (α'') for VODTPA[2]

T (K)	τ_R (s)	α'' (G)	R^2
327	5.95×10^{-11}	3.49	0.98
300	1.05×10^{-10}	0.92	0.99
286	1.56×10^{-10}	0.51	0.99
276	2.08×10^{-10}	0.00	0.98
266	2.90×10^{-10}	0.00	0.97
261	3.82×10^{-09}	2.54	0.96
256	7.19×10^{-09}	1.97	0.98

TABLE 4: Best-Fit Rotational Correlation Times (τ_R) and Residual Line Widths (α'') for VOEOB-DTPA from EPR

T (K)	τ_R (s)	$\alpha''(G)$	R^2
325	1.08×10^{-10}	2.56	0.99
312	1.30×10^{-10}	2.25	0.99
305	1.45×10^{-10}	1.90	0.99
300	1.62×10^{-10}	1.67	0.99
297	1.71×10^{-10}	1.35	0.99
288	2.09×10^{-10}	0.19	0.99
282	2.46×10^{-10}	0.00	0.99
275	3.05×10^{-10}	0.00	0.98

TABLE 5: Best-Fit Rotational Correlation Times (τ_R) and Residual Line Widths (α'') for VOTTHA from EPR

T (K)	τ_R (s)	$\alpha''(G)$	R^2
326	4.57×10^{-11}	2.16	0.99
312	6.00×10^{-11}	2.17	0.99
306	7.00×10^{-11}	2.18	0.99
300	8.72×10^{-11}	2.24	0.99
294	1.15×10^{-10}	0.92	0.99
288	1.41×10^{-10}	1.74	0.99
281	1.87×10^{-10}	1.27	0.99
275	3.33×10^{-10}	6.74	0.98
263	7.13×10^{-09}	4.22	0.97
294[a]	1.20×10^{-10}	0.01	0.97

[a] Q-band result.

Figure 6 shows the Stokes−Einstein plots of the rotational correlation times as functions of temperature and solvent viscosity

$$\tau_R = m\eta/T \tag{6}$$

where m is the slope of the best-fit line to the plot and is:

$$m = 4\pi R^3/3k_B \tag{7}$$

As can be seen from Figure 6, in the region studied, the complexes appear to obey the Stokes−Einstein equation.

The R found here is the hydrodynamic radius. The radius found with this theory usually overestimates the molecular radius; as such the hydrodynamic radius includes the association of the water molecules with the solute molecule.[33] Therefore, the hydrodynamic radius denotes the distance at which the solute molecules are interacting with the water molecules. A zone of interaction can be derived from such a model (indicated by Z in Figure 7) for which water molecules can either form hydrogen bonds with the chelate surface or diffuse closely enough to the agent for hydrodynamic interactions to occur. The hydrodynamic theory assumes that one layer of solvent sticks to the surface of the solute as the solute rotates.[34] Therefore, we can assume that approximately one layer of water is hydrogen-bonded to the second coordination sphere of the complexes.

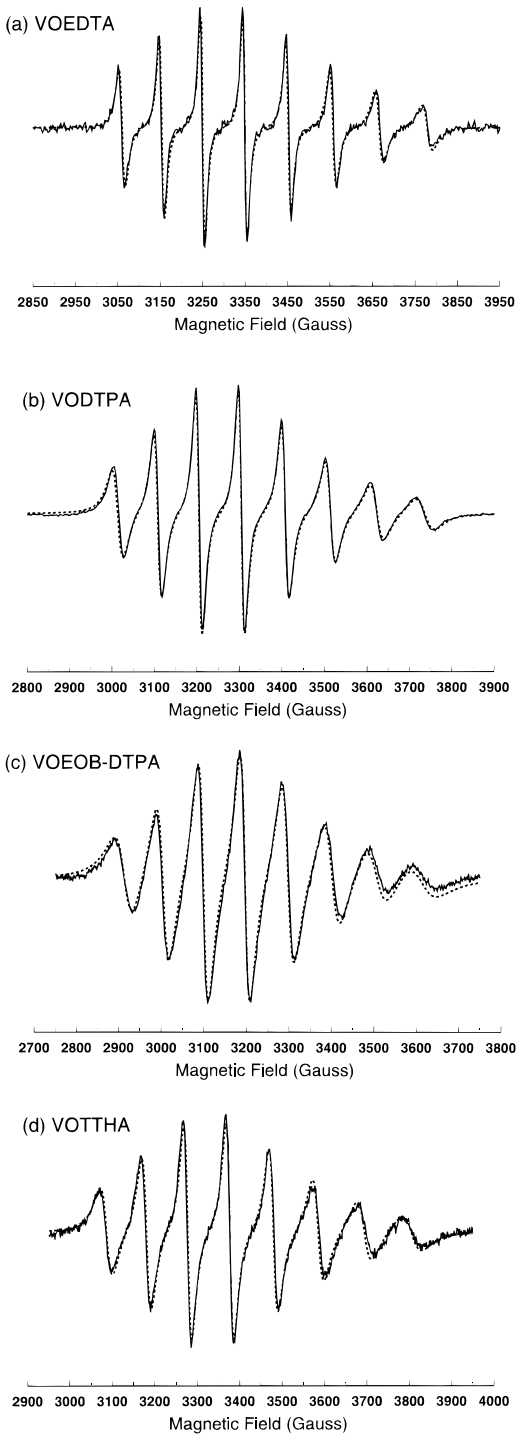

Figure 3. Representative EPR spectra for the four complexes studied in part I. All four spectra shown are at room temperature. The solid lines are experimental spectra while the dashed lines are the best-fit simulation spectra. Note that the larger the complex, the slower it tumbles (and the less it is able to average out the anisotropy in **g** and **A**), resulting in broader lines.

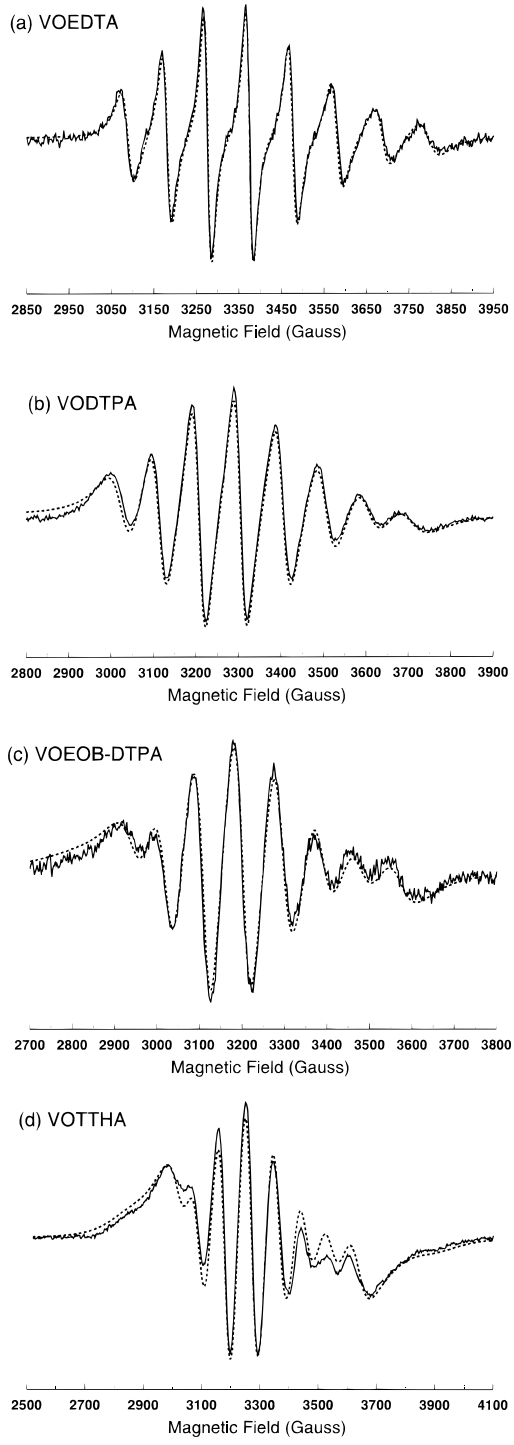

Figure 4. Representative EPR spectra for the four complexes studied in part I. All four spectra shown are at about 275 K. At this temperature, the rotational correlation times are unable to completely average out the anisotropy in **g** and **A**, resulting in greater asymmetry and broader lines than at their respective room temperature counterparts.

The distance of closest approach, or r' (and also a), then can be estimated by accounting for the bond length of O−H in water. Since the normal water O−H bond is 0.958 Å long,[35] one can estimate the distance of closest approach by subtracting ≈0.9 Å from the hydrodynamic radius. The effective distances of closest approach (r') estimated in this fashion are 3.2, 3.8, 4.4, and 4.3 Å for VOEDTA, VODTPA, VOTTHA, and VOEOB-DTPA, respectively.

The physical meaning of the y-intercept of the Stokes−Einstein plot is still lacking.[34] Thus, while the distances

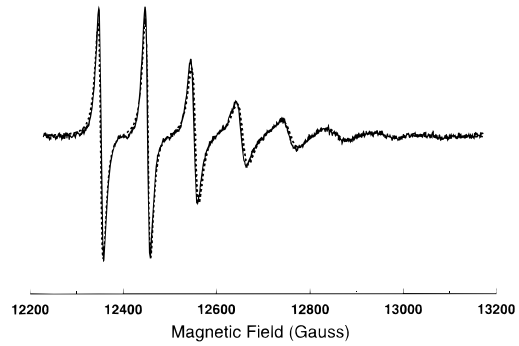

Figure 5. VOTTHA at Q-band, 295 K.

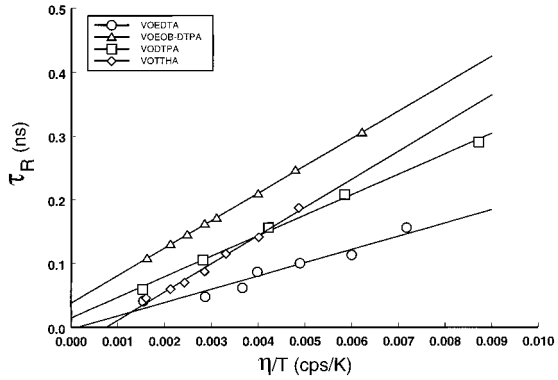

Figure 6. Plot of τ_R vs η/T for the four complexes investigated.

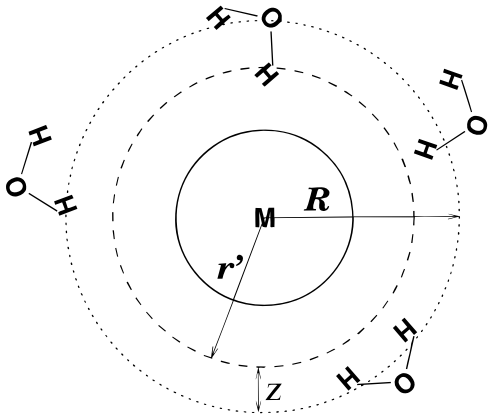

Figure 7. Model used to estimate the distance of closest approach (r') to the metal center (M from the hydrodynamic radius (R) found from EPR). Z is the zone of interaction discussed in the text. The water proton at 12 o'clock indicates one of the water protons at the so-called distance of closest approach.

computed from the EPR data are reasonable, it is not yet clear, for example, why VOTTHA would tumble faster than VODTPA at higher temperatures but slower at lower temperatures, or why VOEOB-DTPA, while similarly sized to VOTTHA, tumbles at a much slower speed. Many factors would complicate a complex's rotational behavior at a given temperature. For example, hydrogen bonding and the ionic character of the complexes would affect substantially a complex's rotational behavior. VOEOB-DTPA has a hydrophobic moiety while VOTTHA may be quite hydrophilic, capable of forming numerous hydrogen bonds. On the other hand, a complex's intramolecular interaction will alter its density and size, thus changing its dynamics relative to other complexes. VOTTHA may be capable of forming a more compact structure around the metal center because it is more flexible. A possible scenario to explain why VOTTHA tumbles faster at higher temperatures but slows down more dramatically than VODTPA at lower

temperatures may be that, at higher temperatures, VOTTHA, having a more compact structure, would tumble slightly faster than VODTPA. However, at lower temperatures, where the complexes tumble slow enough for more hydrogen bonds to form, VOTTHA would be able to attract more water to bind to its surface than the less ionic VODTPA. Interestingly, the smallest chelate, EDTA, does not appear to obey the linearity quite as well as the larger complexes. This may be because EDTA, being smaller and less flexible, deviates more from the spherical symmetry assumed in the hydrodynamic theory presented here. This observation is strengthened by the results of our previous study: we found that in a viscous solution EDTA appears rotationally more anisotropic than does DTPA.[36]

Tables 2−5 also show the residual line widths (α'') for each of the complexes throughout the temperature range studied. The residual line width accounts for contributions from interactions not accounted for by the rotational-modulation of the magnetic tensors and may include unresolved hyperfine interactions and spin-rotational coupling as well as Heisenberg spin exchange. In this study, this "residual line width" was modeled with a Lorentzian line-broadening term in the simulation.[2−4] The excellent agreement between the experimental and the simulated spectra for all the complexes at all the temperatures studied allowed us to avoid adding a Gaussian line-broadening term to the simulation. As shown in the tables, the residual line widths for all the complexes are very small (1−3 G for spectra of 1100 G). This finding, together with the very good fits exemplified by Figure 3, underscores that the isotropic Brownian model is a good model to describe the rotational dynamics of these model complexes. The small increase in α'' near freezing temperatures can be attributed to site-inhomogeneities attendant on the freezing process, while the increase in α'' near the motional-narrowing regime may arise from Heisenberg exchange between vanadyl ions. This is supported by the fact that at intermediate temperatures, where the dynamics of the ions slows down and the exchange process becomes progressively less effective, the residual line width contribution decreases and eventually becomes zero for VODTPA and VOEOB-DTPA. For VOEDTA, we observed a nearly constant, though very small, residual line width contribution. This may be caused by a somewhat less spherical shape of VOEDTA, as evidenced by a small deviation from linearity of its Stokes−Einstein plot (Figure 6). In addition, as mentioned above, we have observed in our sucrose study that VOEDTA in sucrose exhibits larger rotational anisotropy than VODTPA,[36] which again suggests that VOEDTA may not be as spherical as VODTPA, and at the intermediate tumbling rates studied here this rotational anisotropy is not completely averaged out. Since our model assumes a spherical complex, the small residual line width observed could thus be due to a very small rotational anisotropy that is not accounted for in our simulation. For VOEDTA in the motionally narrowed regime, the rotational anisotropy is averaged out, but again Heisenberg exchange may come into play. In the near-rigid limit, site-inhomogeneities from freezing may contribute. Line width trends observed in this work support the data found in Campbell and Freed[4] as well as Chen et al.,[2] but not those reported in Wilson and Kivelson.[3]

3.2. Part II: NMRD of Vanadyl Complexes. 3.2.1. From VOEDTA to VODTPA. Figure 8 shows the NMRD profiles for VOEDTA, VODTPA, and VOEOB-DTPA at various temperatures in the range 278−293 K. Notice that at all temperatures, the relaxivity of VODTPA is higher than that of VOEDTA throughout the entire magnetic field range studied. Since these complexes do not have inner-sphere contributions, either a second-sphere or an outer-sphere model, or possibly both, should be applied to describe the relaxation behavior shown by these profiles.

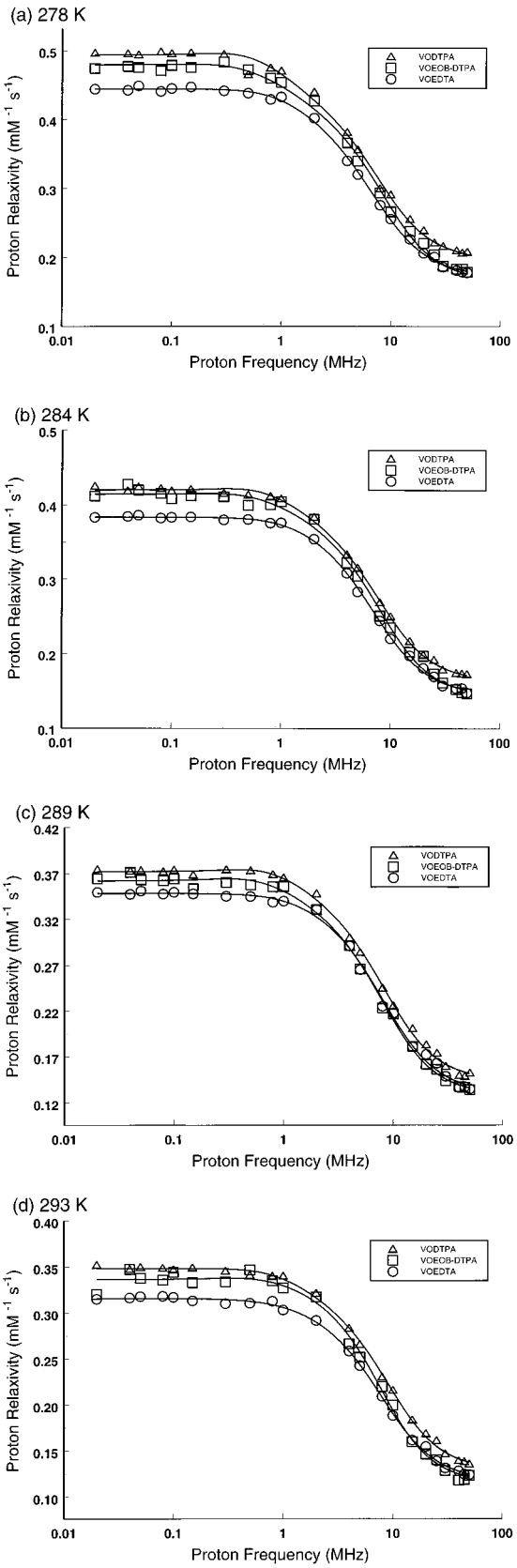

Figure 8. Proton NMRD profiles for VOEDTA, VODTPA and VOEOB-DTPA. The abscissa is $\nu_I = \omega_I/2\pi$. The lines are best-fits utilizing both second-sphere and translational outer-sphere models.

We first considered an outer-sphere mechanism, as is often

TABLE 6: Best-Fit Parameters for VOEDTA under an Outer-Sphere Translational Model[a]

	278 K	284 K	289 K	293 K
τ_{SO} (ps)	150	151	143	150
τ_V (ps)	52	61	53	51
a (Å)	2.02	2.05	2.01	2.10
D (10^{-5} cm^2/s)	2.3	2.7	3.1	3.2

[a] Note that the best-fit a is unphysically small.

TABLE 7: Best-Fit Parameters for VODTPA under an Outer-Sphere Translational Model[a]

	278 K	284 K	289 K	293 K
τ_{SO} (ps)	125	134	131	156
τ_V (ps)	26	43	54	52
a (Å)	1.97	1.99	2.01	2.00
D (10^{-5} cm^2/s)	2.1	2.5	2.8	3.1

[a] Notice that the best-fit a is similar to those those for VOEDTA and unphysically small.

done in literature descriptions of "extra"-inner-sphere relaxivity. The theory used here was presented as eq 3. The distance of closest approach, a, would be larger for VODTPA, as shown in part I. Reasonable values for a (or r' if second-sphere) can be, and have been, estimated from EPR studies (cf. part I). The diffusion coefficient, D, can be computed from the equation:

$$D = D_w + D_x \tag{8}$$

where D_w is the diffusion coefficient of water, and D_x the diffusion coefficient of the paramagnetic complex, and can be estimated using:

$$D_x = k_B T/6\pi\eta a_x \tag{9}$$

These estimated values not only can serve as a starting point for the simulations, but also provide a check of the physical reasonableness of the best-fit parameters.

In this simulation, all four variables in eq 3 are adjustable parameters. The best-fit parameters are given in Tables 6 and 7. While the best-fit values for D are physically reasonable, it is clear from these tables that the values obtained for a are unphysical. The simulation results in unreasonably small distances and gives a values that are about the same for VODTPA and for VOEDTA; in fact, the best-fit a values for VODTPA are actually slightly *smaller* than those for VOEDTA. We attempted to force a to a more reasonable value such as 3 Å, but then the simulation did not converge. Moreover, the quality of the fits is inferior to simulations utilizing a "combined" model (please see Figure 9 and the discussion below). In Bennett et al.,[7] the authors also noted smaller a than that predicted when they attempted to account for their nitroxide NMRD profiles with an outer-sphere-only model. Because possible second-sphere relaxation (see below) was not included in their analysis, they found that they had to inflate the contribution of the outer-sphere process with unphysically small a and D values. These findings suggest that an outer-sphere model, utilizing reasonable values for a and D, would generate a larger relaxation profile for VOEDTA than for VODTPA, contrary to experimental observations. Therefore, an outer-sphere model in which proton relaxation is only modulated by translational diffusion could not adequately account for our observed data.

Is the observed relaxation behavior consistent with a second-sphere model? We have performed EPR studies of VOEDTA and VODTPA in sucrose solutions[36] and have found that an isotropic rotational model does not fit the spectra. An axial

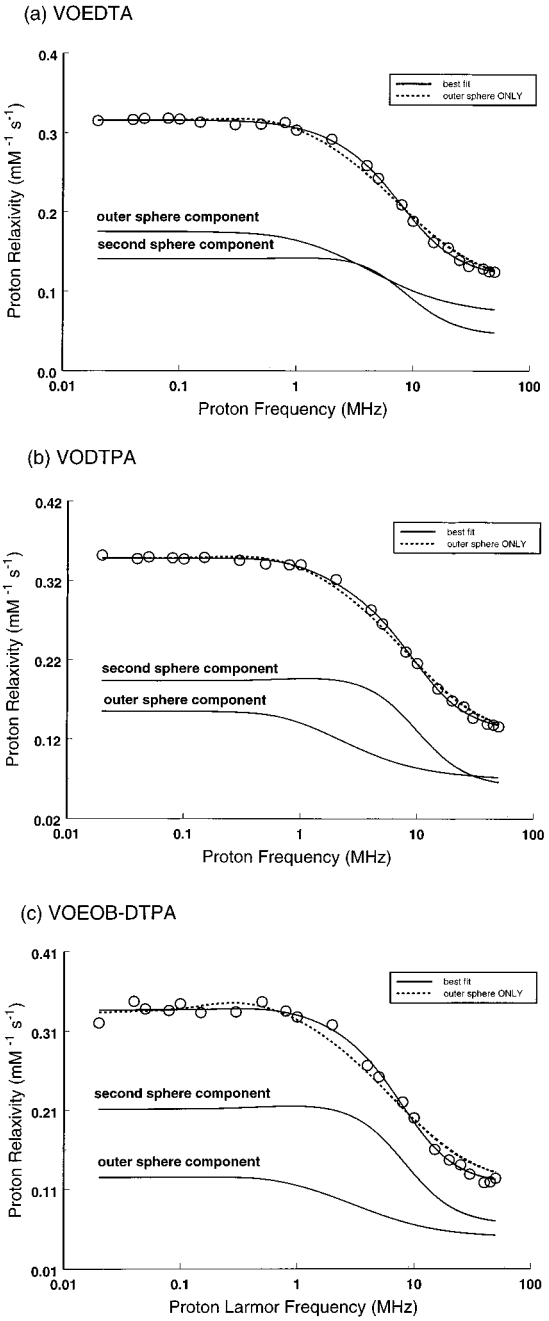

Figure 9. Best-fits of the vanadyl complexes at 293 K. The abscissa is $\nu_I = \omega_I/2\pi$. The solid lines represent the best-fit profiles under the combined second-sphere and outer-sphere models discussed in the text. For comparison, an outer-sphere-only fit is also shown. The bottom two curves of each figure represent the contributions of the second-sphere and the outer-sphere models to the overall relaxivity profile.

anisotropic model describes the spectra much more closely,[36] suggesting that sucrose may bind noncovalently to the second coordination sphere of the complexes. This effectively makes the complexes much less spherical; consequently, the rotational dynamics become anisotropic. This evidence supports the hypothesis that these complexes are capable of forming hydrogen bonds with the solvent molecules and supports the concept of a second coordination sphere.

In this model, where τ_R may be the principal modulator of the total correlation time (τ_C), an increase in τ_R corresponds to an increase in relaxivity (see eq 1). Therefore, from this, one would predict that the larger complex would have a correspondingly larger rotational correlation time and, consequently, a

TABLE 8: Ratios between the Temperatures, the Corresponding Rotational Correlation Times, and the Corresponding High- (50 MHz) and Low- (0.02 MHz) Field Proton Relaxivities for VOEDTA, VODTPA, and VOEOB-DTPA[a]

chelate	T'' (K)/T' (K)	τ_R ratio	R_1 ratio (50 MHz)	R_1 ratio (0.02 MHz)
EDTA	284/278	0.829	0.832	0.862
	289/284	0.862	0.915	0.912
	293/289	0.907	0.921	0.902
DTPA	284/278	0.831	0.833	0.856
	289/284	0.862	0.880	0.881
	293/289	0.908	0.893	0.941
EOB-DTPA	284/278	0.830	0.824	0.868
	289/284	0.878	0.914	0.884
	293/289	0.891	0.922	0.880

[a] The similarity between the ratios is striking and suggests that rotation is the dominant factor modulating the relaxivity of these complexes.

TABLE 9: Best-Fit Results for VOEDTA Proton NMRD Profile Utilizing Both Second-Sphere and Translational Outer-Sphere Models[a]

	278 K	284 K	289 K	293 K
τ_R (ns)	0.11	0.087	0.075	0.068
τ_M' (ps)	6.3	6.5	5.7	5.9
τ_{SO} (ps)	106	96	87	92
τ_V (ps)	26	22	19	17
q'	5.6	5.2	5.6	4.7
D (10^{-5} cm^2/s)	2.2	2.8	3.2	3.4

[a] We have fixed τ_R at the values found by EPR, r' at 3.2 Å, and $\tau_V = \tau_R/4$. The primes on the symbols indicate second-sphere parameters.

higher relaxivity. The actual rotational correlation times have been found from EPR studies in part I (Tables 2 and 3).

Table 8 lists the ratios of τ_R values for the vanadyl complexes studied at successive experimental temperatures as well as the ratios between the low-field (0.02 MHz) relaxivities and the high-field (50 MHz) relaxivities. The ratios of τ_R values correspond well to the high field relaxivity ratios, at which τ_R dominates τ_C for the Solomon−Bloembergen model. Note that at low field, where τ_S and τ_R become similar in magnitude, the relaxivity ratios are still very close to the τ_R ratios, suggesting that τ_R and τ_S may not be independent.[30] Moreover, the observed relaxivity increased as we decreased temperature for each complex, a trend typical of a "τ_R"-limited agent. However, Table 8 reveals that τ_R does not explain all of the relaxivity of these complexes at the various temperatures. Simulations utilizing only a second-sphere model (eq 1) do not fit the profiles any better than those utilizing only the outer-sphere model, and also yield unphysical parameters such as a second-sphere water-proton residence time (τ_M') of nearly a millisecond as well as an extremely large number of second-sphere waters.[2] Both of these findings suggest that the translational diffusion process may still play a role in modulating the relaxivity of these complexes.

Therefore, it is likely that both translational outer-sphere and second-sphere relaxation processes contribute to the observed relaxivity. Simulations utilizing both contributions were performed on the NMRD profiles; the results are shown in Tables 9 and 10 and the best-fit profiles are shown in Figures 8 and 9. Since multidimensional fitting with a large number of parameters may have a simulation landscape with numerous local minima, the EPR results proved invaluable. The results found in part I allowed us to fix four parameters, namely τ_R, τ_V ($\approx \tau_R/4$), r', and a ($= r'$), so that only τ_M', τ_{SO}, q', and D needed to be varied. However, it appeared not to be necessary to fix a under this model as the best-fit a always converged to a value nearly identical with r' (under the constraint that $a \geq r'$). Note that with this model, the NMRD profiles are fitted very closely and yielded physically reasonable parameters for both mechanisms. Figure 9 shows example fits for the complexes at 293 K, along with their respective second-sphere and outer-sphere contributions. For comparison, outer-sphere-only simulations are also shown. Notice that the combined model fits the experimental data more closely than the outer-sphere-only model.

The second-sphere contribution is smaller than the outer-sphere contribution for VOEDTA. This is reasonable since VOEDTA is a smaller complex with fewer functional groups that can attract water protons to coordinate with the second-sphere. Its smaller size also allows water protons to diffuse closer to the metal ion center, accounting for the relatively large outer-sphere contribution. On the other hand, VODTPA is a larger complex with more electronegative functional groups, so it attracts more water protons to the second-sphere while the larger size decreases the relative contribution of the outer-sphere process compared to that of VOEDTA.

Several assumptions in the theory may not be valid for vanadyl complexes. First, **g**, as observed from frozen solution EPR spectra and extracted by SIMPOW, is not isotropic and deviates slightly from axial symmetry (Table 1). Second, molecular tumbling in these complexes, over the temperature range studied, does not completely average out the anisotropy in the spin Hamiltonian. As a matter of fact, it is this incomplete averaging that allows the extraction of accurate rotational correlation times from an EPR study of these vanadyl complexes.[2] Nonetheless, these deviations may not be significant for the interpretation of NMRD profiles since the EPR spectra of these complexes above 5 °C still showed only eight hyperfine lines, though asymmetry and line broadening in line shape are evident even at 50 °C. Third, it is known that τ_R may modulate τ_V and hence τ_S in vanadyl complexes,[30,31] which violates the assumption that the physical processes causing electron and nuclear relaxation be uncorrelated. In addition, it should be noted that it is impossible to separate r', q', and τ_M' (or r, q, and τ_M for inner-sphere relaxation) in the simulation as they are interdependent; varying one changes the other.

Even with these possible violations, the Solomon−Bloembergen model, when combined with the translational diffusion model, describes the experimental profiles better than either model alone. However, since we can no longer assume that the physical processes are uncorrelated, the values found by the simulation may not be the true values, but rather "effective" values as seen through the combined model. However, the simulations are still valuable not because of absolute magnitudes of the best-fit parameters, but rather because of the *relative* magnitudes from one complex to another. Useful information can be obtained by a comparison of the trends exhibited by the best-fit parameters from one complex to another.

The number of second-sphere water ligands, q', is about one per carbonyl oxygen on EDTA, and about three to four per carbonyl oxygen for DTPA. The octadentate DTPA will have three functional groups uncoordinated to vanadyl as compared to one uncoordinated group for the hexadentate EDTA. These additional uncoordinated, electron-dense, groups on DTPA may attract more water ligands. It is also possible that the larger DTPA allows the water to form hydrogen bonds not only with the chelate oxygens but also with each other in close proximity to the paramagnetic ion. The simulation also yielded similar water-proton residence times, τ_M', between the two complexes. This is expected since the two complexes have similar chelate

TABLE 10: Best-Fit Results for VODTPA Proton NMRD Profile Utilizing Both the Second-Sphere and the Translational Outer-Sphere Models[a]

	278 K	284 K	289 K	293 K
τ_R (ns)	0.183	0.152	0.131	0.119
τ_M' (ps)	5.9	5.8	5.5	5.0
τ_{SO} (ps)	136	112	100	113
τ_V (ps)	46	37	33	30
q'	32	30	29	30
D (10^{-5} cm^2/s)	1.6	2.1	2.4	2.8

[a] We have fixed τ_R at the values found by EPR, r' at 3.8 Å, and $\tau_V = \tau_R/4$. The primes on the symbols indicate second-sphere parameters.

TABLE 11: Best-Fit Parameters for VOEOB-DTPA under an Outer-Sphere Translational Model

	278 K	284 K	289 K	293 K
τ_{SO} (ps)	198	231	185	173
τ_V (ps)	98	79	71	111
a (Å)	1.94	1.99	2.08	2.13
D (10^{-5} cm^2/s)	2.4	2.7	2.9	3.0

structures. Since these complexes are not hard spheres, one also would expect some deviations in D as predicted by eqs 7 and 8. From these simulations, second-sphere relaxation is seen to be a significant portion of the "extra"-inner-sphere relaxation, and must be included to describe the relaxation of these complexes.

3.2.2. From VOEDTA and VODTPA to VOEOB-DTPA. Figures 8 and 9 also show the proton relaxivity profiles and the best fits for VOEOB-DTPA at the various temperatures studied. The NMRD profiles show VOEOB-DTPA to have a lower relaxivity than that of VODTPA at low fields and to approach that of VOEDTA at high fields. This is at first surprising in light of the conclusion from the previous section. From EPR studies we have found that VOEOB-DTPA, being the largest of the complexes studied here ($r' \approx 4.3$ Å), tumbles slower than both VOEDTA and VODTPA. Table 4 shows the results from EPR studies. At first glance one would expect a larger relaxivity for VOEOB-DTPA than for VOEDTA and VODTPA because of its slower tumbling rate. That the experiments do not bear out this expectation suggests that another factor not considered in the previous analysis is influencing the relaxivity.

An outer-sphere translational diffusion model could in principle explain the comparison between VODTPA and VOEOB-DTPA. However, this model cannot then explain the increase from VOEDTA to VOEOB-DTPA and cannot explain the observed increase in proton relaxivity between VOEDTA and VODTPA. Therefore, an outer-sphere translational model is not an adequate model to explain the relaxivity differences observed in all three vanadyl complexes. Nonetheless, for comparison, we also fitted VOEOB-DTPA to the translational diffusion outer-sphere model. Best-fit parameters are listed in Table 11. Again, the distance of closest approach, a, is unrealistically small.

Thus, it would appear that neither the second-sphere nor the outer-sphere model adequately explains the observed results. However, the EOB moiety on EOB-DTPA is hydrophobic. This would prevent some water ligands from approaching the second coordination sphere to form hydrogen bonds. Therefore, q', or the number of second-sphere water ligands, would decrease. The addition of the hydrophobic aromatic group on EOB-DTPA will slow τ_R, making the hydrodynamic radius derived from EPR substantially larger than the "effective" distance of closest approach between the water proton and the metal ion. The effective a and r' should be close to that for DTPA since the two chelates are nearly identical in structure. Thus, for the protons to bind to the second coordination sphere of EOB-DTPA complexes, the protons must first penetrate the ethoxybenzyl barrier, and be found near the "DTPA" moiety of EOB-DTPA. Therefore, the NMRD simulation for VOEOB-DTPA used the same r' (3.8 Å) as that of VODTPA.

TABLE 12: Best-Fit Results for VOEOB-DTPA Proton NMRD Profile Utilizing Both the Second-Sphere and the Translational Outer-Sphere Models[a]

	278 K	284 K	289 K	293 K
τ_R (ns)	0.277	0.230	0.202	0.180
τ_M' (ps)	5.2	5.5	5.5	5.9
τ_{SO} (ps)	233	190	151	151
τ_V (ps)	69	58	51	45
q'	38	32	28	27
D (10^{-5} cm^2/s)	2.2	2.8	3.0	3.9

[a] We have fixed τ_R at the values found by EPR, r' at 3.8 Å, and $\tau_V = \tau_R/4$. The primes on the symbols indicate second-sphere parameters.

Using this modification to the second-sphere model, one may expect a decrease in relaxivity for VOEOB-DTPA relative to VODTPA. Note that the outer-sphere model does not take into account the number of protons that may approach the paramagnetic contrast agent and thus does not account for the hydrophobic nature of VOEOB-DTPA. Therefore, only with a second-sphere model could one reconcile this observation in a physically sensible manner. This underscores our conclusion in the previous section that a second coordination sphere contribution must be included in the theory to describe the NMRD profiles of vanadyl complexes. Moreover, as will be shown in part III, the second-sphere model also must be considered when accounting for the NMRD profiles of gadolinium complexes.

Table 12 shows the best-fit parameters for VOEOB-DTPA under the combined model (eqs 1−3, fixing r' at 3.8 Å, as mentioned previously). Figure 9c shows that the outer-sphere contribution to be slightly less than that of VODTPA. This is probably attributable to the EOB moiety keeping bulk water from diffusing past the agent. The number of water ligands actually increased at lower temperatures relative to those for VODTPA. However, recall that VOEOB-DTPA tumbles substantially slower than VODTPA. This allows more water ligands to approach the complex, particularly at the lower temperatures. Comparing the trend shown for q' in Table 12 for VOEOB-DTPA with that in Table 10 for VODTPA, one may infer that at increasingly higher temperatures the hydrophobic moiety would play an increasingly larger role in limiting access to the second coordination sphere.

In addition to exhibiting lower-than-expected relaxivity due to the hydrophobic group, VOEOB-DTPA's NMRD profile also dispersed faster than those for VOEDTA and VODTPA, which dispersed at nearly the same rate. The sharper slope of VOEOB-DTPA at $\omega_I\tau_C \approx 1$ is probably due to the dominance of τ_C by the field-dependent τ_S, since for VOEOB-DTPA, τ_R is large and may not modulate the total correlation time in τ_C.

3.3. Part III: From Vanadyl Complexes to Gadolinium Complexes. Simulations of gadolinium NMRD profiles usually are complicated by the presence of a significant inner-sphere contribution. However, GdTTHA is known to not have any inner-sphere contribution, and a simulation of its NMRD profile based on the model derived for vanadyl complexes (with translational diffusion outer-sphere and second-sphere contributions) is appropriate and useful as a starting point for the more complicated gadolinium complexes. Note that the number of

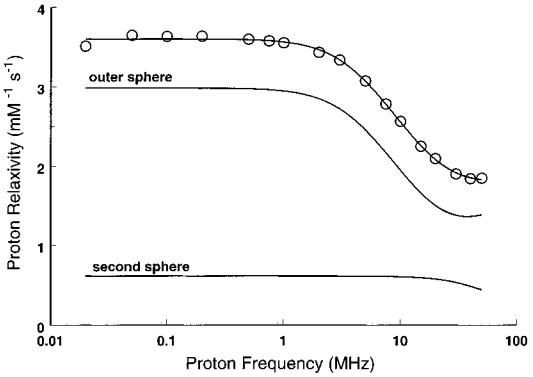

Figure 10. GdTTHA NMRD profile at 293 K and its best-fits under the combined model utilizing both the translational outer-sphere model and the second-sphere model. The abscissa is $\nu_I = \omega_I/2\pi$. The solid line is the second-sphere best-fit (τ_R is fixed at 0.118 ns); best-fit parameters: $\tau_M' = 4.48$ ps, $\tau_{SO} = 81.5$ ps, $\tau_V = 7.52$ ps, $q' = 11.7$, $r' = 4.40$ Å, $a = 4.40$ Å, and $D = 2.05 \times 10^{-5}$ cm^2/s.

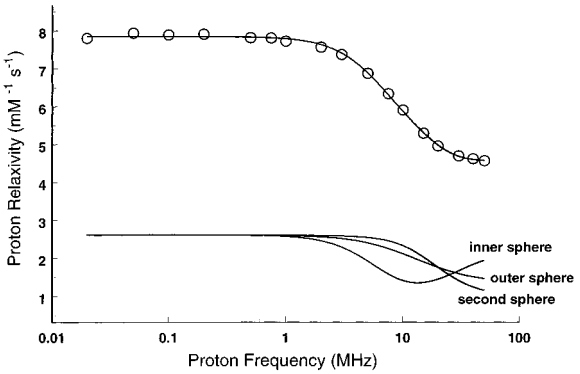

Figure 11. GdDTPA NMRD profile at 293 K and its best-fit. The abscissa is $\nu_I = \omega_I/2\pi$. For both second-sphere and inner-sphere simulations, τ_R is assumed to be the same as that of VODTPA at the same temperature and r' to be the same as derived from EPR for VODTPA; q is assumed to be 1. $\tau_R = 119$ ps, $\tau_M = 20.9$ ns, $\tau_{SO} = 62.7$ ps, $\tau_V = 9.48$ ps, $q = 1$, $r = 3.36$ Å, $\tau_M' = 18.0$ ps, $q' = 6.74$, $r' = 3.80$ Å, $a = 3.80$ Å, and $D = 3.15 \times 10^{-5}$ cm^2/s.

second-sphere water protons, q', for gadolinium complexes is expected to be less than that for the respective vanadyl analogues because gadolinium possesses nine coordination sites (vanadyl has five) and thus will decrease the number of unchelated carbonyl groups that can serve to attract water protons.

Figure 10 shows the best fit under the combined model. GdTTHA has no inner-sphere water (TTHA has 10 chelation groups). The experimental profile is very closely simulated by the theory. The caption for Figure 10 lists the best-fit values found from the simulation for GdTTHA. The approach here is similar to that used for the vanadyl profiles in the previous section. Note that a was not fixed, but still converged to the same value as r'. The best-fit τ_M' of GdTTHA is comparable to the best-fit τ_M' for the vanadyl complexes.

GdTTHA is similar to VOEDTA because both complexes have one unchelated carboxylate group. But they also differ because GdTTHA has many more electronegative groups than VOEDTA due to the difference in the chelates. From both of these observations one would predict that the number of second-sphere waters is slightly larger for GdTTHA than for VOEDTA but smaller than for VODTPA, which has three unchelated groups. The simulation results confirmed this prediction and yielded approximately 12 second-sphere water ligands for GdTTHA, compared to about 7 for VOEDTA and about 30 for VODTPA.

The rotational correlation time was fixed at the value of 118 ps found in the EPR study on VOTTHA from a linear interpolation of the X-band measurements. The distance of closest approach of the second-sphere water ligands, r', also was fixed in the simulations to the value of 4.4 Å derived from VOTTHA EPR measurements (see Table 5). At this distance, the second-sphere contribution diminished dramatically since this dipolar interaction falls off at a rate of r^{-6}. The translational outer-sphere contribution dominates the relaxation profile of GdTTHA. This may be the reason that previous studies found satisfactory fits with a translational diffusion model for the simulation of GdTTHA NMRD profiles. However, for complexes, such as GdDTPA that have smaller distances of closest approach, the second-sphere contribution also would increase proportional to r^{-6}.

To describe complexes with inner-sphere contributions, three more parameters are needed (r, q, τ_M). We fixed the number of inner-sphere water ligands, q, to be *one*, since GdDTPA has one uncoordinated site accessible by water, and τ_R and r' the same values as for VODTPA found in the EPR study shown above and elsewhere.[2,37] Figure 11 shows the best-fit simulation and the caption gives the best-fit values found by the simulation. As predicted from the GdTTHA simulation results, GdDTPA has a relatively larger second-sphere contribution because the water protons can now approach the metal center closer than possible for GdTTHA. The second sphere contributes roughly one-third to the overall relaxivity at low field and decreases slightly to about 25% of the overall relaxivity at the high field. Note that the best-fit τ_M' for GdDTPA is slightly larger than found for GdTTHA and the vanadyl complexes. This may be due in part to the fact that the boundaries for inner- and second-spheres are not necessarily distinct and some mixing between the two zones has occurred; alternatively, because the simulations used similar equations to simulate inner-sphere and second-sphere contributions, we may not be able to completely separate out parameters for each sphere.

The inner-sphere contribution increases dramatically at high fields and actually dominates the overall relaxivity at these higher fields. The simulation clearly demonstrates that at increasingly high fields, inner sphere becomes increasingly more important relative to the other two processes. This explains the increase in relaxivity observed at fields higher than 50 MHz (>1 T). The number of second-sphere water ligands, q', has decreased relative to GdTTHA, in accordance with GdDTPA's having fewer carboxylate groups and no uncoordinated carboxylate group. It is interesting to note that the q' found for GdDTPA in this study ($q' = 6.74$) is similar to the crystallographic result of a similar complex ($q' = 6$).[38] The small difference may be attributed to the difference between solid state and solution phase, as we are observing a dynamic process in this study.

Kellar et al. recently revisited their approach to the simulation of the GdDTPA NMRD profiles.[17] Our best-fit parameter values do not differ qualitatively from theirs in general, but since our approaches differ because we include a second-sphere contribution explicitly in our study, some minor differences are to be expected. Additionally, Kellar et al. apparently used a simplified equation for τ_S; although Kellar et al. did not give their equation for electron relaxation, we reproduced their results exactly if, instead of eq 5, we use[17,18]

$$\tau_S = \tau_{SO}(1+\omega_S^2\tau_V^2) \qquad (10)$$

Nevertheless, where we differ the most are in the values of τ_M and r.

The distance of closest approach for the inner-sphere protons, r, derived in this work for GdDTPA, does not agree with the crystallographic result of 3.06 Å and used in Kellar et al. (3.05 Å).[17] This leads to a smaller inner-sphere contribution than that found in previous studies that do not account for a second-sphere contribution.[14,17] It is important to realize that the r in the SB equations is not a geometric distance, but rather a distance between two point dipoles under the SB model. With this in mind, we have attempted to fix the simulation to 3.06 Å. The resulting best-fit simulation, under our model, yielded poorer fits than that presented in Figure 11 unless we allowed the simulation to use physically unreasonable parameters. While we do not insist that our simulation results represent a perfect simulation of the GdDTPA NMRD profile, we would like to advance the notion that the crystallographic distance, derived from solid-state studies, may not necessarily apply to solutions. There has long been a noted discrepancy, particularly in the field of protein structure, between the distances and structures found from the solid-state crystallographic studies and the solution studies (largely NMR studies). Furthermore, if we fix r to be 3.06 Å but let q vary, then we get fractional q of about 0.6 for the best fit while the relative contributions of the different relaxation regimes are only slightly altered from the presented results. As a matter of fact, if we let both r and q vary, then the best fit occurs at $r \approx 3.2$ Å and $q \approx 0.9$. Clearly, q and r (and τ_M) are interdependent. Therefore, under this model, we found that fixing r' at 3.06 Å is not necessary and does not generate better simulations. Because our simulation algorithm always searches for the best-fit solution, if a larger or smaller contribution from any of the processes would result in a better simulation, the simulation would have found it. Examples of the robustness of our approach are seen in the simulation of GdTTHA, where a rather large outer-sphere contribution gives the best fit, and in the simulation of GdEOB-DTPA, where a large inner-sphere contribution generates the best result; in either case, the second-sphere process contributes relatively smaller fractions to the overall relaxivity. Therefore, we conclude that simulations in which r is allowed to vary do not lead to an underestimation or overestimation of the inner-sphere contribution or any of the other relaxation processes in this work.

It is unlikely that r (likewise r' and a) has a fixed geometric value in solution. From the relaxation point of view, the water-protons will experience inner-sphere relaxation not only at one fixed distance, but also at different distances as they approach the gadolinium. Therefore, the inner sphere is not defined by just one distance, but rather a continuum of distances inside the second and outer-spheres. Because of this, it is probably unreasonable to just plug in geometric distances to reflect the effective relaxation distance for the inner-sphere protons; the effective distance as seen from relaxation is likely to represent an appropriately weighted average over a continuum of distances where the water protons may approach the inner coordination sphere. Our simulations report the best-fit average value of this approach.

Additionally, in this work we constrained q to be 1, an assumption that may not be true, particularly for a system such as EOB-DTPA that restricts the ligand approach and exchange as well as for systems that may form isomers that do not have equivalent water exchange sites. Fractional q may also indicate an equilibrium between $q = 1$ and $q = 0$ species and has been hypothesized and measured in several other works.[37,39] This is possible since on average it is unlikely that every agent will have one water molecule coordinated to it. Additionally, as discussed above, the inner-sphere is not just one distance, so

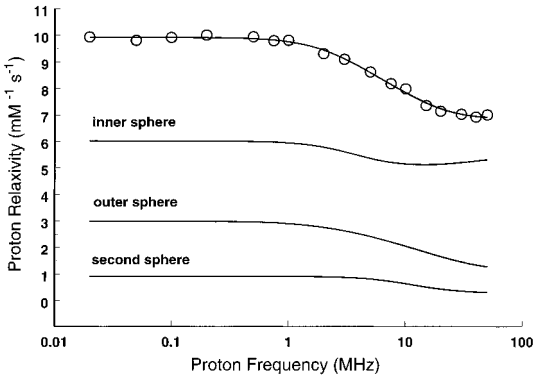

Figure 12. GdEOB-DTPA NMRD profile at 293 K and its best-fit. The abscissa is $\nu_I = \omega_I/2\pi$. For both second-sphere and inner-sphere simulations, τ_R is assumed to be the same as that of VOEOB-DTPA at the same temperature; r' is presumed to be similar to VODTPA/GdDTPA, and q is fixed at 1. $\tau_R = 180$ ps, $\tau_M = 2.73$ μs, $\tau_{SO} = 281$ ps, $\tau_V = 3.59$ ps, $q = 1$, $r = 2.30$ Å, $\tau_M' = 26.0$ ps, $q' = 1.41$, $r' = 3.80$ angstroms, $a = 3.80$ Å, $D = 3.90 \times 10^{-5}$ cm^2/s.

that a better picture is probably one that has a distribution of distances. Therefore, by confining r to one value, fractional q may result. Our best-fit GdDTPA τ_M (water-proton residence lifetime) is 20.9 ns at 293 K. However, please note here that the simulation is in fact insensitive to the magnitude of τ_M because we are not at the regime where $\tau_M > T_{1M}$, i.e., the NMRD profile is not τ_M-limited.[1,14,17,19] As a result of this insensitivity to τ_M, we got nearly equally good fit with a τ_M of 0.3 μs. This value is comparable to the water-oxygen residence lifetime τ_{ex} results found from an ^{17}O NMR study by Micskei and co-workers.[19] Micskei et al. found τ_{ex} to be 240 ns at 298 K.[19] As stated by Micskei et al. and others, τ_{ex} represents the lower limit for the exchange rate for water protons;[1,19] that is, τ_M may not be equal to τ_{ex} (i.e., $\tau_M \leq \tau_{ex}$). Furthermore, τ_M is very sensitive to pH.[40] Micskei and co-workers performed their experiments at pH = 5.3 whereas our experiments were performed at physiologic pH. Therefore, it is important to keep in mind that the values found here and by other studies may in fact all be compatible and reasonable and are different aspects of the same puzzle solved with different techniques from different viewpoints (i.e., from the proton's point of view rather than from the oxygen's point of view).

Figure 12 shows the NMRD profile for GdEOB-DTPA and its deconvolution into second-sphere, outer-sphere, and inner-sphere contributions. We employed the same strategy as before for VOEOB-DTPA: that of fixing the effective distance of closest approach for the second-sphere water protons at 3.8 Å. Again, τ_R was fixed to the value found from EPR for VOEOB-DTPA. The number of second-sphere water ligands decreased to under two because the hydrophobic EOB moiety restricts access to the coordination sites on the second coordination sphere. The second-sphere water-proton residence time is slightly increased relative to the other two gadolinium complexes studied, an effect that may be attributed again to the aromatic moiety that may serve to "trap" the ligand once it penetrated the hydrophobic barrier. Note that this was not observed for VOEOB-DTPA because it has free unchelated carboxylate groups which are not likely to be affected substantially by the EOB moiety. However, for GdEOB-DTPA, because of the presence of the hydrophobic moiety, the second-sphere contribution is 60% smaller than that of GdDTPA, but still roughly 10% of the overall relaxivity.

The inner-sphere simulation yielded an r that is smaller than that for GdDTPA. This could be caused by the EOB's causing strain on the chelating structure, allowing a closer distance of

TABLE 13: Relative Contributions of the Different Relaxation Processes to the Relaxation Profiles of GdDTPA, GdTTHA, and GdEOB-DTPA

	GdDTPA (%)			GdTTHA (%)			GdEOB-DTPA (%)		
frequency (MHz)	inner	second	outer	inner[a]	second	outer	inner	second	outer
0.02	33	33	34	N/A	17	83	61	9	30
20	30	35	35	N/A	28	72	71	6	23
50	43	25	32	N/A	24	76	77	5	18

[a] N/A = not applicable.

approach for the water ligands. This same strain could also contribute to lengthening τ_{SO} and could explain the small dispersion at high fields. This could also be due to the "trapping" effect mentioned above for second-sphere water ligands. The hydrophobic barrier created by the EOB moiety would serve as much to keep water out as to keep it in once the water is already inside the inner coordination sphere. This would lengthen the water-proton residence time as well as shorten the distance of approach.

Note that our model fits the gadolinium profiles slightly more closely than the vanadyl profiles since several assumptions in the SB model possibly violated by vanadyl complexes are valid for gadolinium complexes (**g** is isotropic, no hyperfine interaction, small, if existent, anisotropy only in the zero-field splitting term in the spin Hamiltonian).

It is reassuring to note that in all three complexes, the translational outer-sphere motion contributes nearly the same amount to the relaxation profiles.

It should be mentioned that, as demonstrated by VOEOB-DTPA, using the hydrodynamic radius derived from EPR does not account for the hydrophobic nature of certain chelates. In these cases, electron spin−echo envelope modulation (ESEEM) can be used to find the effective distance of closest approach of the water ligand to the metal ion, albeit only in a rigid medium.[37]

Table 13 lists the relative contribution of each relaxation process to the overall relaxivity profile for GdTTHA, GdDTPA, and GdEOB-DTPA at 0.02, 20, and 50 MHz. While the second-sphere process does not appear to play a large role in the relaxation of GdTTHA and GdEOB-DTPA for reasons already stated, it appears that the second-sphere process is significant in the relaxation of GdDTPA. Therefore, we believe that this indicates that we can further optimize the structures of MRI contrast agents, be they based on gadolinium or other metal centers such as manganese or iron, to take advantage of relaxation enhancement offered by a second coordination sphere.

4. Conclusions

For the vanadyl chelates, although not necessarily for their gadolinium counterparts, the absolute magnitudes of the best-fit parameters found in the NMRD simulations may not represent the true values for these physical processes, as several assumptions of the SBM theory are violated. Nonetheless, by comparing the relative magnitude between the best-fit values of the complexes and looking at the trend exhibited by these values and the experimental profiles, we have demonstrated the importance of second-sphere proton relaxation contribution and found that it may be substantial—more than 30% of the GdDTPA relaxivity. We also have shown that the chelate structure plays a role in determining the second-sphere relaxation contribution, as in EOB-DTPA. So long as we can make the increase in the number of water-ligands larger than the increase in r raised to the negative sixth power, we should see an increase in the second-sphere contribution. This study establishes a basis for designing structural modifications to maximize second-sphere contribution and to increase the relaxivity of future MRI contrast agents.

Acknowledgment. NMR relaxometry was performed at the Magnetic Resonance Laboratory (P41-RR05964, P.C. Lauterbur, P.I.), an NIH Biomedical Research Technology Resource. Most other facilities are provided by the Illinois EPR Research Center, an NIH Biomedical Research Technology Resource (P41-RR01811, R.L. Belford, P.I.). We thank Dr. Radüchel, of Schering, AG, for supplying EOB-DTPA. We thank Dr. Schneider and Prof. Budil for supplying the EPRLF programs and useful discussions. J.W. Chen thanks the University of Illinois Medical School for a summer Hazel I. Craig Fellowship and the U.S. Department of Education for a GAANN Fellowship in Computational Biology. Partial support is provided by the NIH (GM-42208, R.B. Clarkson, P.I.).

References and Notes

(1) Lauffer, R. B. *Chem. Rev.* **1987**, *87*, 901.
(2) Chen, J. W.; Auteri, F. P.; Budil, D. E.; Belford, R. L.; Clarkson, R. B. *J. Phys. Chem.* **1994**, *98*, 13452.
(3) Wilson, L.; Kivelson, D. *J. Chem. Phys.* **1966**, *44*, 154.
(4) Campbell, R. F.; J. H. Freed, J. H. *J. Phys. Chem.* **1980**, *84*, 2666.
(5) Solomon, I. *Phys. Rev.* **1955**, *99*, 559.
(6) Bloembergen, N. J. *J. Chem. Phys.* **1957**, *27*, 572.
(7) Bennett, H. F.; Brown, R. D., III; Koenig, S. H.; Swartz, H. M. *Magn. Reson. Med.* **1987**, *4*, 93.
(8) Kowalewski, J.; Nordenskiöld, L.; Benethis, N.; Westlund, P.-O. *Prog. Nucl. Magn. Reson. Spectrosc.* **1985**, *17*, 141.
(9) Koenig, S. H.: Brown, R. D., III: Lindstrom, T. R. *Biophys. J.* **1981**, *24*, 397.
(10) Bertini, I.: Briganti, F.: Koenig, S. H.: Luchinat, C. *Biochemistry* **1985**, *24*, 6287.
(11) Polnaszek, C. F.; Bryant, R. G. *J. Chem. Phys.* **1984**, *81*, 4038.
(12) Hwang, L.-P.; Freed, J. H. *J. Chem. Phys.* **1975**, *63*, 4017.
(13) Koenig, S. H.; Brown, R. D., III *Prog. Nucl. Magn. Reson. Spectrosc.* **1990**, *22*, 487.
(14) Koenig, S. H. *Magn. Reson. Med.* **1991**, *22*, 183.
(15) Kushnir, T.; Navon, G. *J. Magn. Reson.* **1984**, *56*, 373.
(16) Aime, S.; Botta, M.; Terreno, E.; Lucio Anelli, P.; Uggeri, F. *Magn. Reson. Med.* **1993**, *30*, 583.
(17) Kellar, K. E.; Henrichs, P. M.; Spiller, M.; Koenig, S. H. *Magn. Reson. Med.* **1997**, *37*, 730.
(18) Koenig, S. H.; Brown, R. D., III *NMR Spectroscopy of Cells and Organisms*, Gupta, R. K., ed.; CRC Press: Boca Raton **19**87; Vol. II.
(19) Micskei, K.; Helm, L.; Brücher, E.; Merbach, E. *Inorg. Chem.* **1993**, *32*, 3844.
(20) Chasteen, N. D. Vanadyl(IV) EPR Spin Probes: Inorganic and Biochemical Aspects. *Biological Magnetic Resonance*; Berliner, L. J., Reuben, J., Eds.; Plenum Press: New York, 1981.
(21) To obtain the software at the Illinois EPR Research Center's ftp site use the following steps: (1) ftp ierc.scs.uiuc.edu; (2) at the login prompt type **anonymous**; (3) enter your e-mail address as the password; (4) type **get README.1st** to read what is on the site and where it is located; (5) change directory to the desired directory with the command **cd directory_name**; (6) issue the command **get filename** to get the desired file.
(22) Nilges, M. J. Ph.D. Thesis, University of Illinois, 1979.
(23) Budil, D. E. Personal communcation.
(24) Schneider, D. J.; Freed, J. H. A User's Guide to Slow-Motional ESR Line shape Calculations. *Biological Magnetic Resonance*; Berliner, L. J., Reuben, J., Eds.; Academic Press: New York, 1989; Vol. 8.
(25) Mabbs, F. E.; Collison, D. *Electron Paramagnetic Resonance of d Transition Metal Compounds*; Elsevier: Amsterdam, 1992; Chapter 7.
(26) Brent, R. P. *Algorithms for Minimization without Derivatives*; Prentice Hall: Englewood Cliffs, 1973; Chapter 5.

(27) Nelder, J. A.; Mead, R. *Comput. J.* **1965**, *7*, 308.
(28) Bloembergen, N.; Morgan, L. O. *J. Chem. Phys. 34*, 842.
(29) Koenig, S. H.; Epstein, M. *J. Phys. Chem.* **1975**, *63*, 2279.
(30) Kivelson, D. *J. Chem. Phys.* **1957**, *27*, 1087.
(31) Bertini, I.; Xia, Z.; Luchinat, C. *J. Magn. Reson.* **1992**, *99*, 235.
(32) *Electron Spin Resonance: Elementary Theory and Practical Applications*; Wertz, J. E, Bolton, J. R., Eds.; Chapman and Hall: New York, 1986.
(33) Einstein, A. *Investigations on the Theory of the Brownian Movement*; Dover Publications: 1956; translated by R. Fürth and A. D. Cowper.
(34) Mikosch, W.; Dorfmüller, Th.; Einer, W. *J. Chem. Phys.* **1994**, *101* (12), 11044.
(35) *CRC Handbook of Chemistry and Physics* 67th ed.; Weast, R. C., Astle, M. J., Beyer, W. H., Eds.; CRC Press: Boca Raton, FL, 1986.
(36) Chen, J. W.; Clarkson, R. B.; Belford, R. L. *J. Phys. Chem.* **1996**, *100*, 8093.
(37) Clarkson, R. B.; Hwang, J.-H.; Belford, R. L. *Magn. Reson. Med.* **1993**, *29*, 521.
(38) Konings, M. S.; Dow, W. C.; Love, D. B.; Raymond, K. N.; Quay, S. C.; Rocklage, S. M. *Inorg. Chem.* **1990**, *29*, 1488.
(39) Aime, S.; Botta, M.; Parker, D.; Williams, J.A.G. *J. Chem. Soc., Dalton Trans.* **1996**, *1*, 17.
(40) Meiboom, S. *J. Chem. Phys.* **1961**, *34*, 375.